### Title

Enhancements of residual Reynolds stresses by magnetic perturbations in the edge plasmas of the J-TEXT tokamak




### Journal

Nuclear Fusion, 60(10)

### ISSN

0029-5515



### Authors

Zhao, KJ
Chen, ZP
Shi, Yuejiang
et al.



### Publication Date

2020-10-01

### DOI

10.1088/1741-4326/abadad

# Enhancements of residual Reynolds stresses with magnetic perturbation in the edge plasmas of the J-TEXT tokamak

# Enhancements of residual Reynolds stresses with magnetic perturbation in the edge plasmas of the J-TEXT tokamak

*K. J. Zhao[1], Z. P. Chen[2], Yuejiang. Shi[3], P. H. Diamond[4], J. Q. Dong[5], Z. Y. Chen,[2] Y. H. Ding,[2] G. Zhuang,[2] Y. B. Liu[1], H. Q. Zhang[1], Y. Q. Chen[1], H. Liu,[2] J. Cheng,[6] L. Nie,[1] B. Rao,[2] Z. F. Cheng,[2] L. Gao,[2] X. Q. Zhang,[2] Z. J. Yang,[2] N. C. Wang,[2] L. Wang,[2] J. Q. Li[5], W. Jin,[2] J. Q. Xu,[1] L. W. Yan,[1] Y.F. Liang[2], Y. Y. Xie[1], B. Liu[6] and J-TEXT team[2]*

1. *School of Nuclear Science and Engineer, East China University of Technology, 330013, Nanchang, China*
2. *International Joint Research Laboratory of Magnetic Confinement Fusion and Plasma Physics, State Key Laboratory of Advanced Electromagnetic Engineering and Technology, School of Electrical and Electronic Engineering, Huazhong University of Science and Technology, 430074, Wuhan, China*
3. *ENN Science and Technology Development Co., Ltd., Langfang, Hebei 065001, China*
4. *Center for Momentum Transport and Flow Organization, University of California at San Diego, California, 92093, USA*
5. *Southwestern Institute of Physics, 610041, Chengdu, China*
6. *Institute of Fusion Science, School of Physical Science and Technology, Southwest Jiaotong University, 610031, Chengdu, China*

**Abstract:** The enhancements of the residual Reynolds stresses and symmetry breaking with resonant magnetic perturbations (RMPs) are presented. These experiments were performed using a Langmuir probe array in the edge plasmas of the J-TEXT tokamak. This study aims at understanding the generating mechanisms of residual stresses and intrinsic rotations. It is observed that, with RMPs, the peaked residual stresses, steeper pressure gradients and stronger shear layers all appear around the resonant surface. The toroidal rotation is accelerated in the direction of the

plasma current and shows correlation with turbulence and the measured residual stresses near the resonant surfaces of RMPs. The symmetry breaking induced by magnetic islands is proposed as a new mechanism. It qualitatively explains the enhanced residual stresses and the acceleration of the toroidal rotation. The changes of the residual stresses and the symmetry breaking with RMPs near the last closed surface are also discussed.

PACS numbers: 52. 35. Ra, 52. 25. Fi, 52. 35. Mw, 52. 55. Fa

## 1. Introduction

Interaction of magnetohydrodynamic (MHD) structures and flows has attracted much attention, such as angular momentum transport in astrophysical disks [1, 2], dynamics of the earth core and geodynamo [3] and magnetic braking of stellar rotation [4]. In fusion plasmas, the study of interactions between plasma flows and magnetic structure aims at understanding and controlling plasma confinement and transport [5-8]. Resonant magnetic perturbations (RMPs) have significant effects on cross field transport and plasma profiles [9–20], and are widely used to mitigate/suppress the large scale edge - localized mode (ELM) in tokamak plasmas [20].

It is widely accepted that the toroidal rotation is an important player for improving plasma confinement [21-22] and stabilizing MHD modes [23-24] in tokamaks and in helical devices. The toroidal rotation can be generated by external momentum input, such as neutral beam injection. It can also be formed spontaneously/intrinsically without apparently momentum input [25-30]. The intrinsic rotation is considered to be induced by residual Reynolds stresses via turbulence. The residual stress is a part of the total Reynolds stress which can be described as $\langle \delta v_r \delta v_\emptyset \rangle = -D_{ff} \frac{\partial \langle V_\emptyset \rangle}{\partial r} + V_{pin} \langle V_\emptyset \rangle + R_{resi}$, where $\langle \delta v_r \delta v_\emptyset \rangle$ is the total Reynolds stress, $-D_{ff} \frac{\partial \langle V_\emptyset \rangle}{\partial r}$ refers to the diffusive stress, $V_{pin} \langle V_\emptyset \rangle$ and $R_{resi}$ are the pinch and residual stresses, respectively. The residual stress is independence of the averaged

velocity and velocity gradient, and only depends on the characteristics of turbulence, the gradient of temperature, density and pressure etc. Considering that the contribution of the momentum pinch term disappears for the flow driving, the poloidal residual stress was observed in a linear machine [25]. Cancelling the intrinsic rotation using neutral beam injection, the residual stress was also detected on TEXTOR [31]. A possible mechanism is the ***EXB*** shear flow effect on symmetry braking of turbulence that contributes to the generation of the residual stress [26]. This mechanism has been discussed in Ohmic plasmas [31].

When applying RMPs, the coherent magnetic islands and stochastic magnetic fields will be generated in plasmas. The RMP-induced magnetic island and stochastic regions have strong effects on the plasma flows and turbulence [13-19, 32]. Generally speaking, the radial electric field $E_r$ increases in magnetic island and stochastic regions [15, 17-18, 33 - 34]. In some cases, the braking effects on the toroidal rotation due to RMPs were measured in the core plasmas [35]. There are also some cases, showing that the toroidal rotation is accelerated with RMPs. The co- and counter-current toroidal rotations are accelerated by deeply penetrating RMPs of m/n = 3/1 mode configuration [36] and by RMPs with small injected neutral beam momentum [37], respectively. The acceleration of the toroidal rotation due to RMPs was also observed in tokamak edge plasmas [19, 32-34]. The correlation between the acceleration of toroidal rotations and turbulence with RMPs has been examined [19]. In addition, the phase relationship between the plasma edge density and electron temperature is well correlated with the relative rotation of the RMP field and the toroidal rotation [38]. However, to understand the underlying physics of the RMP effects on toroidal rotation, the residual stress and its generation mechanism with RMPs should be studied in experiments.

Here, the residual Reynolds stress, pressure gradients, ***EXB*** flow shears and symmetry breaking in tokamak edge plasmas with RMPs are presented. It is shown that the residual stresses, pressure gradients and flow shears are varied significantly around the resonant surface of RMPs. The residual stress is well correlated with the increased toroidal rotation in the direction of the plasma current and turbulence

around the resonant surface when the RMP coils are applied. The analysis reveals that the RMPs may break the turbulence symmetry and induce the residual stress and thus intrinsic rotation. The residual stress and the symmetry breaking near the last closed flux surface (LCFS) are also discussed with and without RMPs.

The rest of this work is organized as follows. The experimental set-up is given in section 2. The experimental results with RMPs, described in section 3, include the radial distributions of the edge plasma parameters, the estimation of turbulence diffusive stresses, total Reynolds stresses and residual stresses, free energy for residual stress, flow shears on symmetry breaking and RMP – induced island effects on symmetry breaking etc. Section 4 presents the conclusion and discussion.

## 2. Experiment setup

The experiments presented here were conducted in ohmic plasmas with circular cross section on the J-TEXT tokamak. The major and minor radii of the J-TEXT tokamak are R = 1.05 m and a = 0.255 m, respectively [39]. The plasma parameters for the experiments are the toroidal magnetic field $B_t$ = 1.9 - 2.0 T, the plasma current $I_p$ = 150 - 160 kA, the line averaged electron density $N_e$ = 1 – 2 x $10^{19} m^{-3}$, and the edge safety factor $q_a$ = 4.1 - 4.3. A set of coils, called a dynamic RMP, has been installed inside the vessel on J-TEXT to study the interaction between helical perturbations and magnetized plasmas, and explore a possible method for control of tearing modes [40-41]. In the present study, the static configuration of RMP was used. The base mode and strength of the magnetic perturbation were varied by adjusting the power supply to the coils. The perturbation field strength of ~ 1.16 x$10^{-5}$ T for m/n = 4/1 mode can be obtained for 1kA in the coils assuming no plasma response. Here, m

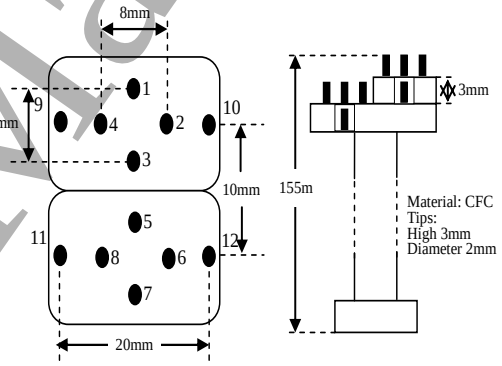


Fig 1 (color online) Configuration of a fast reciprocating probe array. ($V_f$: 1, 3, 5, 7; $V_+$: 4, 8; $V_-$: 2, 6; $I_{s\text{-}up}$: 10, 12; $I_{s\text{-}down}$: 9, 10.)

and n are the poloidal and toroidal mode numbers, respectively. The maximum RMP current is 6.5 kA. A fast reciprocating probe array with two steps and 12 tips as shown in figure 1 yields the profiles of floating potential, temperature, density, Mach number etc. It was mounted on the top of the tokamak. The length and diameter of the tips are 3 mm and 2 mm, respectively. The digitizer can handle fluctuation data up to 2 MHz.

Figures 2(a) and (b) give the time periods of the RMP current and line average density for two shots 1035477 and 1035476 with and without RMPs, respectively. With RMPs, the density changes slightly. This suggests that there is no significant degradation for the plasma confinement with RMPs. The probe scans the plasma parameters during the RMP current flat. Figures 2(c) - (d) describe the displacement of the Mach probe array, floating potential fluctuations and sheath current collected on Mach probe tips at the up-stream sides, respectively. The $\Delta r$ refers to the distance from the measurement point to the last closed flux surface (LCFS) and minus means inside the LCFS. When the probes stay inside the plasmas stably, the average floating potential (the average sheath current) is ~110V (~0.35A).

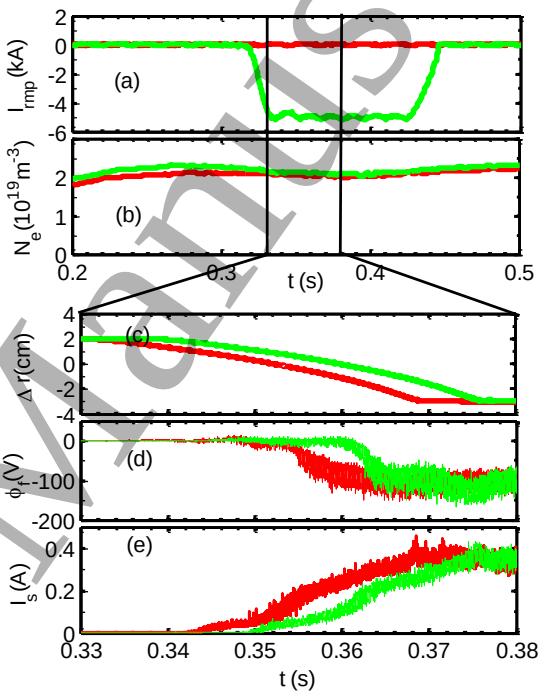


Fig 2 (a) RMP currents, (b) line average density, (c) displacement of the reciprocating probe array, (d) floating potential fluctuations and (e) sheath currents at the up-stream sides for shots 1035477 (green) and 1035476(red) with and without RMPs, respectively.

## 3 Experiment results

### 3.1 Radial distributions of edge plasma parameters with and without RMPs

The radial profiles of the edge parameters inside the LCFS are measured in Ohmic plasmas with and without RMPs. The RMP current is ~5kA and produces a

relative magnetic perturbation $\delta B_r/B_0$ ~ 3 x $10^{-5}$ for the m/n = 4/1 mode without considering the plasma response. The plasma rotation is detected using a Mach probe array. The Mach numbers are evaluated as $M_{mach} = 0.4 \ln (I_{s\text{-}up}/ I_{s\text{-}down})$, where $I_{s\text{-}up}$ and $I_{s\text{-}down}$ refer to the sheath currents collected on two Mach probe tips at the up- and down-stream sides, respectively. Based on the estimated Mach number and the measured electron temperature, the toroidal velocity can be obtained as $V_\varphi \approx M_{mach} C_s$. The $C_s$ is ion sound speed as $\sim \sqrt{2T_e / m_i}$, here $T_e$ and $m_i$ are the electron temperature and the ion mass, respectively. The radial electric field $E_r$ can be calculated from the plasma potential. The plasma potential is evaluated from the measured temperature ($T_e$) and floating potential ($\phi_f$) as $\phi_{pl} \sim \phi_f + 2.5\ T_e$.

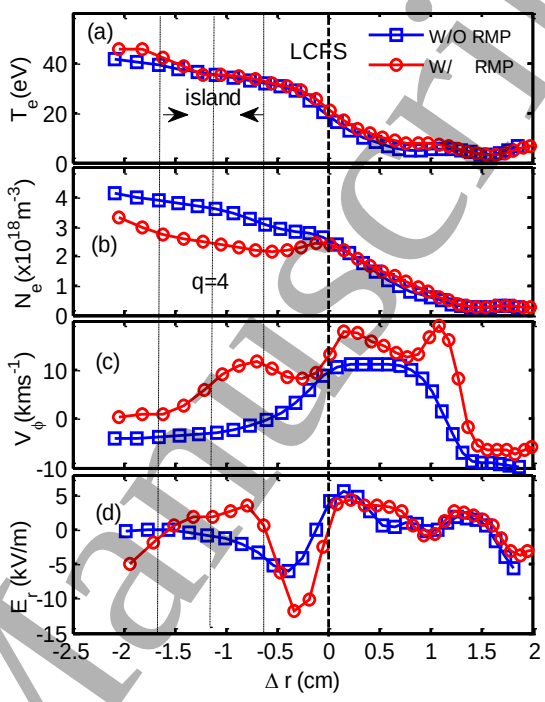


Fig 3 The radial profiles of (a) electron temperature, (b) electron density, (c) toroidal rotation velocity and (d) radial electric field in the edge plasmas with and without RMPs [$I_p$ = 150 kA, $B_t$ = 2.0T, $N_e$ = 2.0x$10^{19}$ $m^{-3}$, $q_a$ = 4.3].

Figures 3 (a) - (d) present the radial dependences of the electron temperature, electron density, toroidal rotation velocity and radial electric field at $q_a$ = 4.3 (shots:1035476 and 1035477), respectively. Compared with the cases without RMPs, the electron temperature almost does not change while the electron density in the interval -1.7 < $\Delta$r < - 0.7 cm decreases significantly with RMPs. The decrease of the electron density attributes to the occurrence of the magnetic islands in the interval -1.7 < $\Delta$r < - 0.7cm. The island width $w$ is proportional to $\delta B_r^{1/2}$ and estimated as ~1cm. This is consistent with the flat profile of the density. The resonant surface is evaluated

from the magnetic measurement. However, the flat effect is not significant for the electron temperature. The possible reason is that the island with width of ~1cm is relatively small. Steeper gradients of the electron temperature and density all appear near the LCFS in both cases with and without RMPs. Without RMPs, the steeper toroidal velocity gradient appears near the LCFS. The evolutions of the toroidal velocities in the scrape-off layer possibly come from the effects of the secondary limiter at $\Delta r$ ~ 1.0 cm due to the RMP assembly. We will not discuss this more in detail and the RMP effects on the residual stress and **ExB** shear flows near the LCFS and the resonant layers will be focused on in this paper. The positive and negative signs of the toroidal velocities indicate that the plasmas rotate in the co- and counter - current directions, respectively. Compared with the cases without RMPs, the toroidal rotations increase in almost all the edge area with RMPs, especially in the interval -1.2 < $\Delta$ r < -0.7cm. The rapid increase of the toroidal rotation is observed not only near the LCFS but also in the q = 4 resonant layers with RMPs. Moreover, the reversal of the toroidal rotation is observed in the interval -2.0 < $\Delta r$ < -0.5cm and its sign changes from the counter-current direction to the co-current direction. The $E_r$ increases near the q = 4 resonant surfaces due to the existence of the magnetic islands with RMPs. The decrease of the $E_r$ suggests that a stronger $E_r$ shear layer forms near the LCFS with RMPs. In addition, a peak in density profiles appears near the LCFS. This may come from the stronger shear layer formation near the LCFS because of the

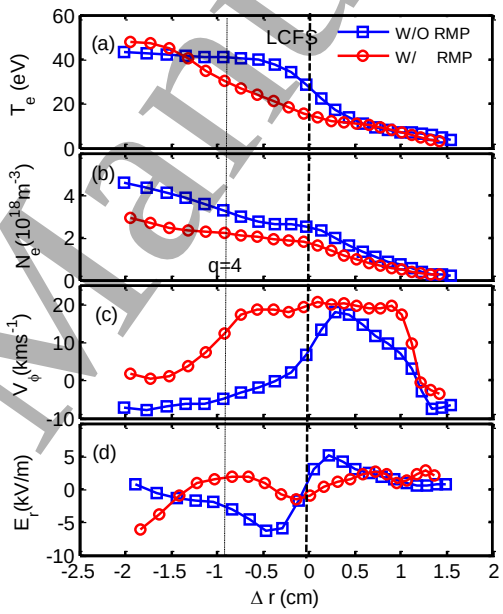


Fig. 4 The radial profiles of (a) electron temperature, (b) electron density, (c) toroidal rotation and (d) radial electric field in the edge plasmas with and without m/n = 4/1 RMPs [$I_p$ = 150 kA, $B_t$ = 1.9 T, $N_e$ = 2.0 x $10^{19}$ $m^{-3}$, $q_a$ = 4.1].

occurrence of the magnetic islands.

The edge plasma parameters are also detected with and without RMPs at $q_a = 4.1$. Figures 4 (a) - (d) show the radial distributions of the electron temperature, electron density, toroidal rotation velocity and radial electric field (shots:1035469 and 1035478), respectively. With RMPs, the shapes of the plasma profiles at $q_a = 4.1$ significantly differ from those in the cases at $q_a = 4.3$. The steeper gradient of the $T_e$ appears near the q = 4 resonant surface while the $T_e$ becomes flattened near the LCFS with RMPs. The appearance of the steeper gradient of the $T_e$ might come from that the q = 4 resonant layer is closer to the LCFS so that the RMP - induced islands touch the limiter, or a stochastic region forms. Compared with the cases without RMPs, the density significantly decreases in the interval $-2.0 < \Delta r < 0.5$cm with RMPs and is consistent with the cases at $q_a = 4.3$. Similar to the cases at $q_a = 4.3$, the toroidal rotation is also significantly accelerated around the q = 4 resonant layer with RMPs. With RMPs, the $E_r$ also increases near q = 4 surface and its sign changes from negative to positive at $q_a = 4.1$. This is also similar to those observed in the cases at $q_a = 4.3$. However, the flat $E_r$ appears near the LCFS with RMPs at $q_a = 4.1$, i.e., decreases outside the LCFS and increases inside the LCFS.

Note that RMP-induced island can be distinguished from the stochastic region although there are somehow similarities inside the island and stochastic regions in some physics. The reason is that the reversal of magnetic field occurs at O-point of the island, but not at the center of the stochastic region. This suggests that some physics are different at two sides of the O-point [8,17]. For example, the sign of island-induced flows reverses at O-point. In the following analysis, the reversal of the gradient of the Reynolds stress at O-point will be presented. This indicates that the sign of the flows induced by Reynolds stress itself reverses inside the islands. Therefore, the stochastic region is not discussed further in this paper.

Based on the observation, it is revealed that the mutual interaction between edge plasmas and RMPs show the complicated characteristics. The changes of the profiles attribute to not only the RMPs but also the location of the resonant surface. Next, relating to the intrinsic rotation generation, the residual stress and its driving

mechanisms will be discussed.

### 3.2 Diffusive stresses with and without RMPs

To get the residual stresses, the diffusive stresses are estimated here in advance. The diffusive stresses are expected as $-D_{ff}\frac{\partial\langle V_\emptyset\rangle}{\partial r}$, where the $D_{ff}$ is the turbulent momentum diffusivity and the $\frac{\partial\langle V_\emptyset\rangle}{\partial r}$ means the gradient of the toroidal velocity. The $D_{ff}$ can be calculated as $\langle\delta v_r^2\rangle t_c$, here the $\langle\delta v_r^2\rangle$ and $t_c$ are the mean - squared radial turbulent velocity and the turbulent autocorrelation time, respectively.

Figures 5 (a) - (d) show that the radial distributions of (a) the turbulent autocorrelation time, (b) the mean squared radial turbulent velocity, (c) turbulent

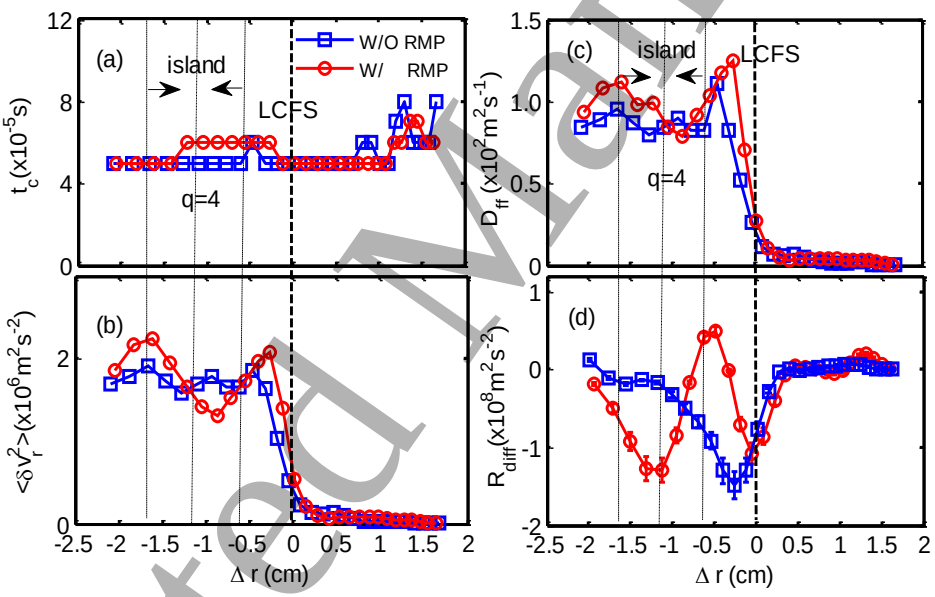


Fig. 5 Radial profiles of (a) turbulent autocorrelation time, (b) mean-squared radial turbulent velocity, (c) turbulent momentum diffusivity and (d) diffusive stresses with and without RMPs at $q_a$=4.3.

momentum diffusivity and (d) diffusive stresses with and without RMPs at $q_a$ = 4.3, respectively. Turbulent correlation time almost keeps constant in the interval -2.0 < $\Delta$ r < 1cm without RMPs while it varies slightly near the q = 4 resonant surfaces with RMPs. The steeper gradient of the $\langle\delta v_r^2\rangle$ is found to appear near the LCFS with and without RMPs. However, the $\langle\delta v_r^2\rangle$ profiles are significantly different near the

resonant surface with and without RMPs, i.e., the $\langle \delta v_r^2 \rangle$ is flat without RMPs while a $\langle \delta v_r^2 \rangle$ well forms due to the magnetic island with RMPs. This is consistent with the previous observation, i.e., turbulence intensity drops inside the magnetic island and increase at its boundaries [17]. The shapes of the turbulent momentum diffusivity profiles are similar to those of the $\langle \delta v_r^2 \rangle$ with and without RMPs. The calculated diffusive stress drops and shows a big negative peak near the LCFS without RMPs. In contrary, with RMPs, two big negative peaks appear and are located near the LCFS and the resonant surfaces.

The diffusive stresses are also measured with and without RMPs at $q_a$ = 4.1.

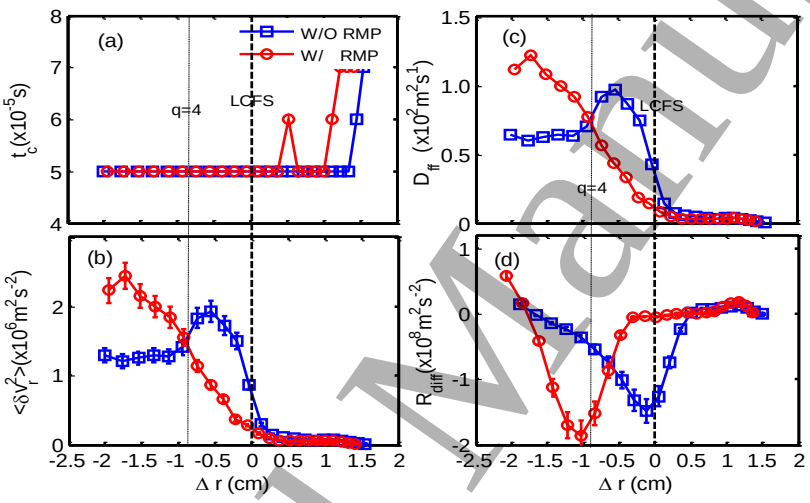


Fig. 6 Radial profiles of (a) turbulent autocorrelation time, (b) mean-squared radial turbulent velocity, (c) turbulent momentum diffusivity and (d) diffusive stresses with and without RMPs at $q_a$ = 4.1.

Figures 6 (a) - (d) describe that the radial dependences of (a) the turbulent autocorrelation time, (b) the mean squared radial turbulent velocity, (c) turbulent momentum diffusivity and (d) diffusive stresses with and without RMPs at $q_a$ = 4.1, respectively. The evaluated correlation time of the turbulence is constant in the interval -2.0 < Δ r < 0.5cm with and without RMPs. Without RMPs, significant turbulence collapse is observed near the LCFS and similar to those observed in the cases at $q_a$ = 4.3. With RMPs, the steeper gradient of the $\langle \delta v_r^2 \rangle$ moves to the q = 4 resonant surfaces. This differs from the cases at $q_a$ = 4.3, where a $\langle \delta v_r^2 \rangle$ well occurs. The shape of the $D_{ff}$ profiles is also similar to that of the $\langle \delta v_r^2 \rangle$ with and without

RMPs. The negative peak of the diffusive stress also appears near the LCFS without RMPs. However, the negative peak disappears near the LCFS and is presented near the resonant surface with RMPs. This is significantly different from the measurements at $q_a$ = 4.3, i.e., two negative peaks are located near the LCFS and the resonant surface.

As a result of the change of the radial profiles of turbulence and toroidal rotation, turbulence diffusive stress is significantly varied near the resonant surface and LCFS with RMPs. Note that in steady state plasmas, the diffusive stress should balance the residual stress.

### 3.3 Residual stresses with and without RMPs

In steady state plasmas, the total Reynolds stress effect is not significant and turbulence momentum pinch is considered to be small for driving toroidal rotation. Thus, it is reasonable to assume $\langle \delta v_r \delta v_\emptyset \rangle \sim 0$ and $V_{pin}\langle V_\emptyset \rangle \sim 0$, then the residual stresses can be calculated as $R_{resi} = D_{ff}\frac{\partial \langle V_\emptyset \rangle}{\partial r}$, i.e., the residual stress is balanced by the diffusive stresses, as mentioned above. Next, the total Reynolds stress and residual stress will be estimated with and without RMPs.

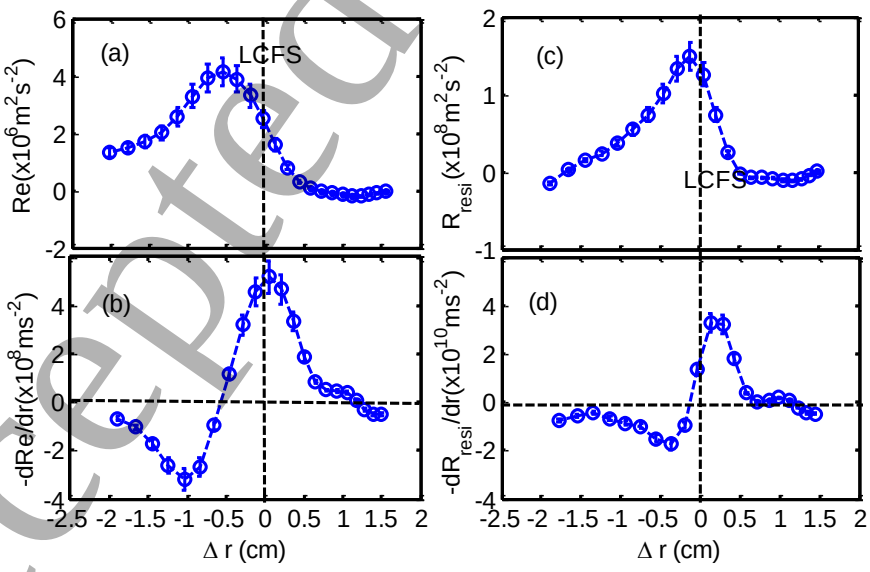


Fig. 7 The radial distributions of (a) total Reynolds stress and (b) corresponding gradient, and (c) residual stress and (d) corresponding gradient without RMPs at $q_a$ = 4.1.

Figures 7 (a) and (b) give the radial distributions of the total Reynolds stress $Re = \langle \delta v_r \delta v_\emptyset \rangle$ and corresponding gradient $-\frac{d(Re)}{dr} = -d(\langle \delta v_r \delta v_\emptyset \rangle)/dr$ without RMPs at $q_a$ = 4.1, respectively. The Reynolds stress is determined by the amplitudes of $\delta v_r$, $\delta v_\emptyset$ and their correlation (or cross phase). The steep gradient of the $Re$ and a positive peak of the $-d(Re)/dr$ appear near the LCFS. The evaluated residual stress and its gradient are shown in figures 7 (c) and (d), respectively. The steep gradient of the $R_{resi}$ and a positive peak of the $-d(R_{resi})/dr$ also occur near the LCFS. This is consistent with the measurement of the toroidal rotation, i.e., the toroidal rotation rapidly goes up and reaches maximum near the LCFS without RMPs. The positive (negative) Reynolds stress force accelerates the co-current (counter-current) toroidal rotation on J-TEXT. However, there is no significant counter-current toroidal rotation which appears at the negative peak of the $-d(R_{resi})/dr$. The possible reason is the flow damping and that the intrinsic rotation commonly is considered to be generated at the edge and propagate inward. Note that without RMPs, only intrinsic rotation is generated. This observation suggests that the residual stress exists and plays an important role in driving toroidal rotations.

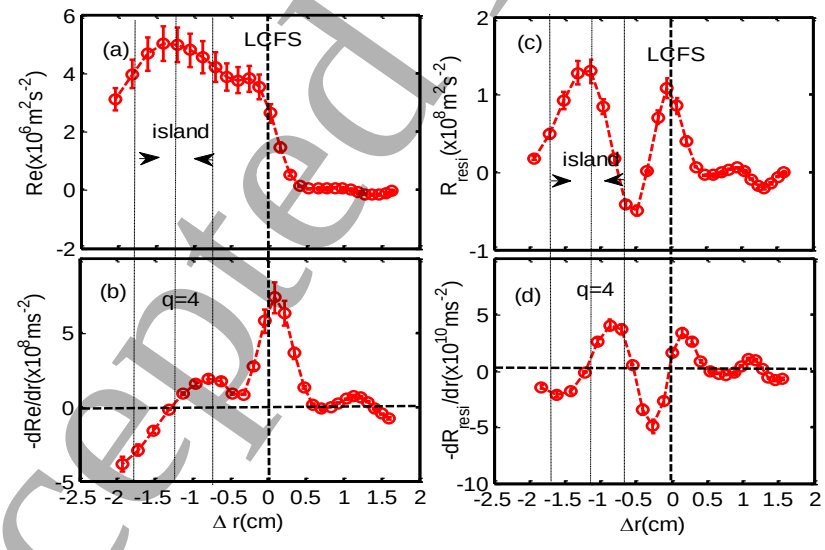


Fig. 8 The radial distributions of (a) total Reynolds stress and (b) corresponding gradient, and (c) residual stress and (d) corresponding gradient with RMPs at $q_a$ = 4.3.

The radial distributions of the total Reynolds stress and corresponding gradient with RMPs at $q_a$ = 4.3 are presented in figures 8 (a) and (b), respectively. The total Reynolds stress rapidly reduces and a big positive peak of its gradient appears near the LCFS. This observation is similar to the measurements without RMP at $q_a$ = 4.1. However, the significant total Reynolds stress and its gradient also occur in the magnetic island region. The residual stress and its gradients are given in figures 8(c) and (d), respectively. Two big positive peaks of the residual stresses appear in the magnetic island region and near the LCFS. The significant positive gradient of the residual stresses is observed at the outer side of the resonant surface and near the LCFS. This is consistent with the increase of the co-current toroidal rotation near the resonant surface and LCFS with RMPs at $q_a$ = 4.3. Similar to the cases without RMPs, the counter-current toroidal rotation is not observed at the negative peak of the $-d(R_{resi})/dr$ near the resonant surface and the LCFS. This result suggests that the intrinsic rotation can be generated at the outer side of the q = 4 surface and near the LCFS, and propagate inward.

To understand the RMP effects on the toroidal rotation, the radial profiles of the total Reynolds stress and its gradient are shown in figures 9 (a) and (b) with RMPs at $q_a$ = 4.1, respectively. The stress profile becomes flat near the LCFS and the steeper gradient of the stresses also occur near the resonant surface. The radial distributions of

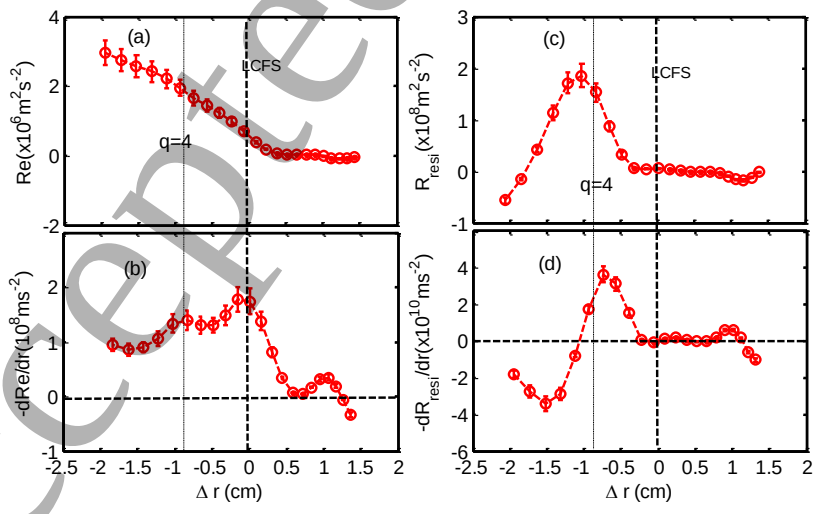


Fig. 9 The radial distributions of (a) total Reynolds stress and (b) corresponding gradient, and (c) residual stress and (d) corresponding gradient with RMPs at $q_a$ = 4.1.

the residual stresses and its gradient are given in figures 9 (c) and (d), respectively. Compared with the cases without RMPs and at $q_a = 4.3$ with RMPs, the peak of the residual stress disappears due to the flat profiles of the diffusive stresses and moves to the $q_a = 4.0$ resonant surface. The positive peak of the gradient of the residual stress also moves to the outer side of the resonant surface and is in line with the increase of the toroidal rotation near the resonant surface. Similarly, the negative gradient of the residual stress does not correspond to the negative toroidal rotation near the resonant surface. Note that the co-current toroidal rotation is still accelerated near the LCFS with RMPs at $q_a = 4.1$ although the peak of the residual stress and its gradient disappear. This suggests that except for the residual stress, other factors may also play dominant role on the toroidal rotation.

The measured residual stress is about two orders of the magnitude greater than the total Reynolds stress with and without RMPs. This indicates that the total Reynolds stress is negligible and the derivation of $R_{resi}$ is justified based on the experiment data. The residual stress is enhanced and shows correlation with the toroidal rotation near the resonant surface with RMPs.

### 3.4 Free energy for the residual stresses with and without RMPs

Normally, the turbulent Reynolds stress is considered to be driven by the free energy of the pressure gradient. However, magnetic structures, such as magnetic islands, can also release free energy. To understand the observed residual stress and toroidal rotation, the origin of the free energy with RMPs is discussed.

Figures 10 (a) - (b) describe the radial distributions of the electron pressure $P_e$ and corresponding gradient $P_e'$ with and without RMPs at $q_a = 4.3$, respectively. Note that the ion pressure profile is not shown here. Assuming that the ion temperature is equal to the electron temperature, the ion and electron pressure profiles are identical. The pressure and its gradient do not vary significantly near the LCFS with and without RMPs. This suggests the free energy for the stress is still provided by the pressure gradients near the LCFS with RMPs at $q_a = 4.3$. However, inside the LCFS, the pressure significantly decreases with RMPs. Meanwhile, the pressure gradient

becomes steeper (flat) at inner (outer) side of the resonant surface. This observation suggests that the RMP- induced island changes the pressure gradient. However, we note that the residual stress peak occurs inside the island and the toroidal rotation is driven in the outer side of the resonant surface dominantly. This is in contradiction with that the steeper pressure gradient is localized in the inner side of the resonant surface. The observation suggests that the free energy for the stresses around the resonant surface does not comes from the pressure gradient and one possibility is from the islands due to the RMPs.

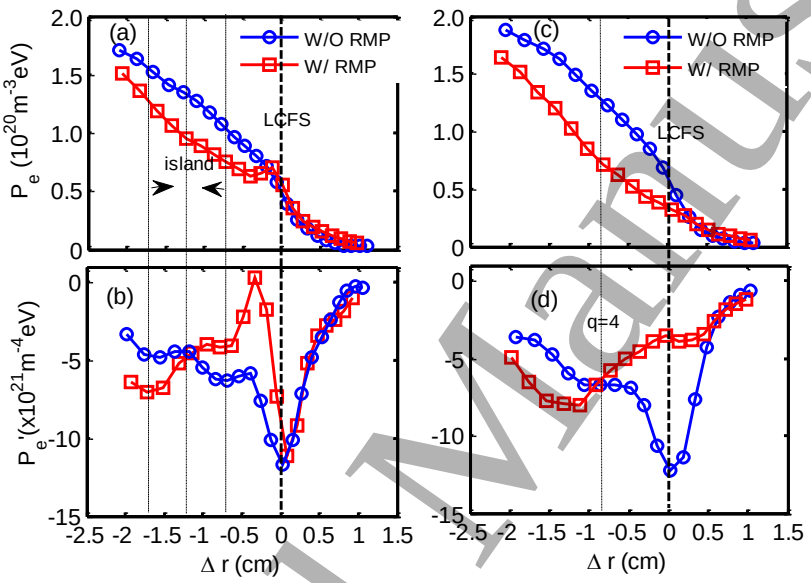


Fig. 10 The radial distributions of (a) electron pressure and (b) corresponding gradient with and without RMPs at $q_a$=4.3, and (c) electron pressure and (d) corresponding gradient with and without RMPs at $q_a$ = 4.1.

The radial profile of the pressure gradient with RMPs are also examined at $q_a$=4.1. The electron pressure and corresponding gradient are presented in figures 10 (b) and (c) with and without RMPs, respectively. Similar to the cases at $q_a$= 4.3, the reduction of the pressure appears inside the LCFS and the steeper (fatter) gradient is localized at inner (outer) side of the resonant surface at $q_a$ = 4.1. However, the residual stress peak (a rapid increase in the toroidal rotation) is also localized near (at the outer side of) the resonant surface. This result is similar to the observation at $q_a$=4.3 with RMPs, i.e, the free energy for the stress around the resonant surface is not provided by the pressure

gradient and possibly origins from the magnetic islands. Near the LCFS, the gradient is flattened significantly and the peaked residual stress disappears with RMPs at $q_a$ = 4.1. This differs from those observed in the cases with RMPs at $q_a$= 4.3, where the free energy results from the pressure gradient.

The observation suggests that with RMPs, the free energy to drive the residual Reynolds stresses can be provided by magnetic island near the resonant surface and by the pressure gradient near the LCFS. Moving towards the LCFS, the steeper gradient and peaked residual stress disappear near the LCFS.

### 3.5 *ExB* flow shears on symmetry breaking with and without RMPs

The $k_{\|}$ symmetry breaking is required for the residual stress and intrinsic rotation generations, here $k_{\|}$ is the parallel wave vector. The breaking of $k_{\|}$ symmetry with respect to 0 point can result in that the spectrally averaged $\langle k_{\|} \rangle$ is nonzero. A possible mechanism of symmetry breaking is the $E_r$xB shear flows and the $R_{resi}$ is proportional to $E_r'$, here $E_r'$ is the $E_r$xB shearing rates. Generally, the shear flows can shift the centroid of the fluctuation spectrum through tearing and tilting the turbulent eddies, and thus break the symmetry. Consequently, the Reynolds stress $\langle \delta v_r \delta v_{||} \rangle$ is generated.

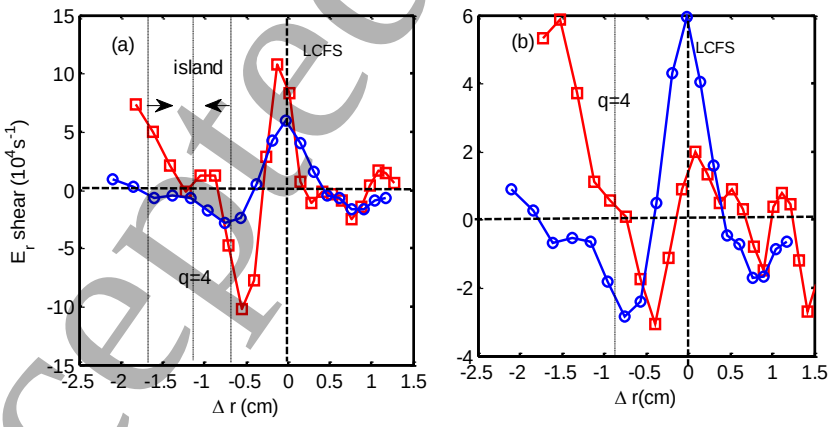


Fig. 11 The radial distributions of $E_r$ shearing rates with and without RMP at $q_a$ = 4.3 (a) and 4.1 (b).

For understanding the underlying physics of the rotation and residual stress, the

$E_r$xB shearing rates are calculated with and without RMPs. The radial profiles of the shearing rates at $q_a = 4.3$ are given in figure 11(a). Near the LCFS, the higher shearing rates occur for both cases with and without RMPs. This is in line with the measurement, i.e., the significant residual stress, the increase of the toroidal rotation and the steeper pressure gradients are localized near the LCFS with and without RMPs at $q_a = 4.3$. The observation suggests that the effects of the $E_r$xB shear on the symmetry breaking play dominant role on the residual stress and the toroidal rotation near the LCFS with and without RMPs at $q_a = 4.3$.

However, the shearing rates are significantly different around the resonant surface for two cases as shown in Fig 11 (a). For the cases without RMPs, the shearing rates close to zero at the resonant surface. With RMPs, the shearing rates are higher at the boundaries of the island. This is not consistent with that the residual stress peak appears inside the islands. The result indicates that the enhanced residual stress around the resonant surface cannot be explained by the $E_r$xB flow shear effects on symmetry breaking.

The $E_r$xB flow shears on symmetry breaking are examined further with RMPs through varying the edge safety factors. The shearing rates are evaluated at $q_a = 4.1$ with and without RMPs as shown in figure 11(b). Similarly, the shearing rates are significantly varied with RMPs. Compared with the cases at $q_a = 4.3$, with RMPs, the shearing rate drops near the LCFS. This is in line with the flat profiles of residual stress near the LCFS with RMPs at $q_a$=4.1. However, stronger flow shears also exist at the inner and outer sides of the $q_a = 4$ surface. This is also not in agreement with the observations of the peaked residual stress around the resonant surface with RMPs at $q_a = 4.1$

The measurement suggests that the peaked residual stress near the LCFS with and without RMPs is induced by the EXB flow shears on the symmetry breaking. However, the symmetry breaking of the turbulence around the resonant surface cannot attribute to the observed flow shears. The possible reason is that the symmetry breaking might be induced by magnetic islands.

### 3.6 RMP -induced island effects on symmetry breaking

A new mechanism of symmetry breaking, which is induced by magnetic islands, is suggested to understand the present observations of the residual stress and flow shears with RMPs. The island effects on symmetry breaking can be simply seen from the derivation of the correlator of the residual stress. The residual stress is proportional to the $\langle k_\theta k_{||}\rangle$ and can be written as $R_{resi}\sim\langle k_\theta k_{||}\rangle\langle\delta\varphi^2\rangle$, where the $k_\theta$ is the poloidal wave number and $\langle k_\theta k_{||}\rangle$ is the correlator. It is clear that the nonzero $\langle k_\theta k_{||}\rangle$ is necessary for the generation of the residual stress and induced by symmetry breaking. The $k_{||}=\frac{\boldsymbol{k}.(\boldsymbol{\delta B}+\boldsymbol{B_0})}{|B_0|}=\frac{\boldsymbol{k}.\boldsymbol{B_0}}{|B_0|}+\frac{\boldsymbol{k}.\boldsymbol{\delta B}}{|B_0|}=k_{||,0}+\delta k_{||}$, where $\boldsymbol{B_0}(\boldsymbol{\delta B})$ is equilibrium （fluctuation） magnetic field and the bold black indicates vectors, so that the correlator $\langle k_\theta k_{||}\rangle=\langle k_\theta k_{||,0}\rangle+\langle k_\theta\delta k_{||}\rangle$. Considering the equilibrium symmetry, $\langle k_\theta k_{||,0}\rangle=0$ and $\delta k_{||}=\frac{k_\theta\delta B_\theta+k_\varphi\delta B_\varphi}{|B_0|}$, here $\delta B_\theta$ $(\delta B_\varphi)$ is the poloidal (toroidal) magnetic fluctuation and $k_\varphi$ is the toroidal wave number, then the equation $\langle k_\theta k_{||}\rangle=\langle k_\theta\delta k_{||}\rangle=\langle k_\theta^2\rangle\frac{\delta B_\theta}{|B_0|}+\langle k_\theta k_\varphi\rangle\frac{\delta B_\varphi}{|B_0|}$ is easy to be obtained. Thus, the residual stress can be rewritten as $R_{resi}\sim\langle k_\theta^2\rangle\frac{\delta B_\theta}{|B_0|}\langle\delta\varphi^2\rangle$ due to $\langle k_\theta k_\varphi\rangle=0$. It is obvious that the $\delta B_\theta$ can play an important role on the symmetry breaking and then residual stress. Generally speaking, the maximal value of the $\delta B_\theta$ is localized at the O-points for magnetic islands. This analysis is qualitatively consistent with the measurements, i.e., the peaked residual stress is observed around the resonant surface with RMPs.

## 4. Conclusion and discussion

The enhancement of residual Reynolds stress and symmetry breaking with resonant magnetic perturbations are studied in the edge plasmas of the J-TEXT tokamak. Without RMPs, the peaked residual stresses, steeper pressure gradients, stronger flow shears and accelerated toroidal rotation all appear near the LCFS. This result is consistent with that the symmetry breaking induced by flow shears

contributes to the generation of the residual stress and intrinsic rotation. Compared with the cases without RMPs, the residual stress peaks, steeper gradients, enhanced flow shears and acceleration of the toroidal rotation all occur near not only the LCFS but also the resonant surface with RMPs at $q_a = 4.3$. Near the LCFS, those profiles are also in accordance with that the residual stress and intrinsic rotation attribute to the flow shear effect on symmetry breaking of turbulence. However, the peaked residual stress does not correspond to the steeper pressure gradient and stronger flow shear around the resonant surface. Similar results around the resonant surface are also obtained with RMPs at $q_a = 4.1$. Such symmetry breaking cannot be explained by flow shears. An alternative explanation is the island effect on symmetry breaking. In addition, with RMPs at $q_a = 4.1$, the peaked residual stress is not observed near the LCFS where the toroidal rotation is accelerated. The result indicates that other factors may drive the toroidal rotation near the LCFS with RMPs at $q_a = 4.1$.

Note that the effects of the total Reynolds stress and pinch term are considered to be negligible for the measurement of the residual stress in this experiment. The estimated total Reynolds stress is small enough and satisfies our assumption. Usually, it is difficult to measure the pinch term directly in experiment. However, in general, the pinch stress is far less than the diffusive stress in the regime of the steep toroidal rotation in steady state plasmas [42 - 43].

The Residual stress near the resonant surface is first investigated with RMPs. This study suggests that the symmetry breaking due to RMPs - induced islands may contribute to the residual stress and thus toroidal rotation.

**Acknowledgements:** This work is supported by East China University of Technology, High level introduction of talent research start-up fund No. 1410000993, and Doctoral start-up fund No. DHBK2018059; by National Science Foundation of China, Nos. 11775069, 11320101005 and 11705151; by Landmark achievements in nuclear science and technology No. xxkjs2018011and by Jiangxi provincial key research and development plan, No. 20192ACB80006.

**Reference**

[1] Balbus S. A. and Hawley J. F. 1991 *Astrophys. J.* **376** 241.

[2] Balbus S. A. and Hawley J. F. 1998 *Rev. Mod. Phys.* **70** 1.

[3] Aubert J. and Fournier A. 2011 *Nonlinear Process. Geophys.***18** 657.

[4] Matt S. *et al* 2012 *Astrophys. J. Lett.* **754** L26.

[5] Hu Z.Q. *et al 2014 Nucl. Fusion 54 123018.*

[6] Hu Z.Q. *et al 2016 Nucl. Fusion 56 016012.*

[7] Zhao K J *et al* 2016, *Phys. Rev. Lett. 117,145002.*

[8] Zhao K. J *et al* 2017, *Nucl. Fusion 57,126006.*

[9] Unterberg B. *et al* 2009 *J. Nucl. Mater.* **390–1** 351.

[10] Schmitz O. *et al* 2009 *J. Nucl. Mater.* **390** 330.

[11] Jakubowski M.W. *et al* 2006 *Phys. Rev. Lett.* **96** 035004.

[12] Schmitz O. *et al* 2012 *Nucl. Fusion* **52** 043005.

[13] Ida K. *et al* 2001 *Phys. Rev. Lett.* **88** 015002.

[14] Finken K.H. *et al* 2007 *Nucl. Fusion* **47** 522.

[15] Xu Y. *et al* 2006 *Phys. Rev. Lett.* **97** 165003.

[16] Leconte M. and Diamond P.H. 2012 *Phys. Plasmas* **19** 055903.

[17] Zhao K.J. *et al* 2015 *Nucl. Fusion* **55** 073022.

[18] Xu Y. *et al* 2007 *Nucl. Fusion* **47** 1696.

[19] Zhao. K.J et al., 2016, *Nucl. Fusion* **56** 076005.

[20] Evans T.E. *et al* 2004 *Phys. Rev. Lett.* **92** 235003.

[21] Rice J.E. *et al* 2004 *Nucl. Fusion* **44** 379.

[22] Rice J.E. *et al* 1999 *Nucl. Fusion* **39** 1175.

[23] Berkery J.W. *et al* 2010 *Phys. Rev. Lett.* **104** 035003.

[24] Takechi M. *et al* 2007 *Phys. Rev. Lett.* **98** 055002.

[25] Yan Z. *et al* 2010 *Phys. Rev. Lett.* **104** 065002.

[26] Diamond P.H. *et al* 2013 *Nucl. Fusion* **53** 104019.

[27] Rice J.E. *et al* 2007 *Nucl. Fusion* **47** 1618.

[28] Rice J.E. *et al* 2011 *Phys. Rev. Lett.* **106** 215001.

[29] Yoshida M. *et al* 2008 *Phys. Rev. Lett.* **100** 105002.

[30] Shi Y.J. *et al* 2011 *Phys. Rev. Lett.* **106** 235001.

[31] Xu Y. *et al* 2013 *Nucl. Fusion* **53** 072071.

[32] Tamain P. *et al* 2010 *Plasma Phys. Control. Fusion.* **52** 075017.

[33] Unterberg B. *et al* 2007 *J. Nucl. Mater.* **363–5** 698.

[34] Coenen J.W. *et al* 2011 *Nucl. Fusion* **51** 063030.

[35] LaHaye R.J. *et al* 1994 *Phys. Plasmas* **1** 373.

[36] Finken K.H. *et al* 2005 *Phys. Rev. Lett.* **94** 015003.

[37] Garofalo A.M. *et al* 2008 *Phys. Rev. Lett.* **101** 195005.

[38] Stoschus H. *et al* 2010 *Phys. Plasmas* **17** 060702.

[39] Zhuang G. *et al* 2011 *Nucl. Fusion* **51** 094020.

[40] Rao B. *et al* 2014 *Fusion Eng. Des.* **89** 378.

[41] Tang W. K *et al* 2020 *Nucl. Fusion* **60** 026015.

[42] Diamond P H *et al* 2009 *Nucl. Fusion* **49** 045002.

[43] Hahm T S *et al 2007 Phys. Plasmas*,**14**, 072302.